

# Synchrotron Emission from VHE Gamma-Ray Induced Pair Cascades in AGN Environments

P. Roustazadeh and M. Böttcher<sup>1</sup>

## ABSTRACT

The discovery of very-high-energy (VHE,  $E > 100$  GeV)  $\gamma$ -ray emission from intermediate- and low-frequency peaked blazars suggests that  $\gamma\gamma$  absorption and pair cascading might occur in those objects. In previous papers, we investigated the Compton emission from VHE  $\gamma$ -ray induced pair cascades, deflected by moderate magnetic fields, in a largely model-independent way, and demonstrated that this emission can explain the Fermi fluxes and spectra of the radio galaxies Cen A and NGC 1275. In this paper, we describe a generalization of our Monte-Carlo cascade code to include the angle-dependent synchrotron output from the cascades, allowing for the application to situations with non-negligible magnetic fields, leading to potentially observable synchrotron signatures, but still not dominating the radiative energy loss of cascade particles. We confirm that the synchrotron radiation from the cascades in NGC 1275 and Cen A are negligible for the parameters used in our previous works. We demonstrate that the magnetic field can not be determined from a fit of the cascade emission to the  $\gamma$ -ray spectrum alone, and the degeneracy can only be lifted if the synchrotron emission from the cascades is observed as well. We illustrate this fact with the example of NGC 1275. We point out that the cascade synchrotron emission may produce spectral features in the same energy range in which the big blue bump is observed in the spectral energy distributions of several blazars, and may make a non-negligible contribution to this feature. We illustrate this idea with the example of 3C 279.

*Subject headings:* galaxies: active — galaxies: jets — gamma-rays: galaxies — radiation mechanisms: non-thermal — relativistic processes

---

<sup>1</sup>Astrophysical Institute, Department of Physics and Astronomy,  
Ohio University, Athens, OH 45701, USA

## 1. Introduction

Among AGNs, blazars are the most luminous and violent objects in the universe and emit  $\gamma$ -rays at energies higher than 100 MeV. They are divided into two main subgroups: Highly variable quasars, sometimes called optically violent variable (OVV) quasars, and BL Lacertae objects (BL Lac). Since one of the jets of blazars is pointed toward the Earth, we see the jet emission strongly Doppler enhanced and highly variable. According to the unification scheme (Urry & Padovani 1995), radio galaxies are the mis-aligned parent population of blazars. Synchrotron peak frequencies of BL Lac objects cover a large range from IR to X-rays, and based on its location they are called low-frequency peaked BL Lac objects (LBL; synchrotron peak in the IR), intermediate BL Lac objects (IBL; synchrotron peak in the optical/UV), or high-frequency peaked BL Lac objects (HBL; synchrotron peak in the X-rays).

While there is little evidence for dense radiation environments in the nuclear regions of BL Lac objects — in particular, HBLs —, strong line emission in Flat Spectrum Radio Quasars (FSRQs) as well as the occasional detection of emission lines in the spectra of some BL Lac objects (e.g., Vermeulen et al. 1995) indicates dense nuclear radiation fields in those objects. This is supported by spectral modeling of the SEDs of blazars using leptonic models which prefer scenarios based on external radiation fields as sources for Compton scattering to produce the high-energy radiation in FSRQs, LBLs and also some IBLs (e.g., Ghisellini et al. 1998; Madejski et al. 1999; Böttcher & Bloom 2000; Acciari et al. 2008; Abdo et al. 2011). If the VHE  $\gamma$ -ray emission is indeed produced in the high-radiation-density environment of the broad line region (BLR) and/or the dust torus of an AGN, it is expected to be strongly attenuated by  $\gamma\gamma$  pair production (e.g. Protheroe & Biermann 1997; Donea & Protheroe 2003; Reimer 2007; Liu et al. 2008; Sitarek & Bednarek 2008). Aharonian et al. (2008) have suggested that such intrinsic  $\gamma\gamma$  absorption may be responsible for producing the unexpectedly hard intrinsic (i.e., after correction for  $\gamma\gamma$  absorption by the extragalactic background light) VHE  $\gamma$ -ray spectra of some blazars at relatively high redshift. A similar effect has been invoked by Poutanen & Stern (2010) to explain the spectral breaks in the *Fermi* spectra of  $\gamma$ -ray blazars. This absorption process will lead to the development of Compton-supported pair cascades in the circumnuclear environment (e.g., Bednarek & Kirk 1995; Sitarek & Bednarek 2010; Roustazadeh & Böttcher 2010, 2011).

In Roustazadeh & Böttcher (2010, 2011), we considered the full 3-dimensional development of Compton-supported VHE  $\gamma$ -ray induced cascades in the external radiation fields in AGN environments. In those works, we have left the origin (leptonic SSC or IC, or hadronic) of the primary VHE  $\gamma$ -ray emission deliberately unspecified in order to investigate the cascade development in as model-independent a way as possible. We have shown that even

very weak magnetic fields ( $B \lesssim \mu\text{G}$ ) may be sufficient for efficient quasi-isotropization of the cascade emission. We applied this idea to fit the *Fermi*  $\gamma$ -ray emission of the radio galaxies NGC 1275 and Cen A. In Roustazadeh & Böttcher (2010, 2011), parameters were chosen such that the synchrotron emission from the cascades was negligible.

In this paper, we present a generalization of the Monte-Carlo cascade code developed in Roustazadeh & Böttcher (2011) to non-negligible magnetic fields and consider the angle dependent synchrotron emission from the cascades. In section 2, we will outline the general model setup and assumptions and describe the modified Monte-Carlo code. Numerical results for generic parameters will be presented in section 3. We confirm that for the objects Cen A and NGC 1275 the synchrotron radiation from the cascades is negligible for those parameters used in Roustazadeh & Böttcher (2010, 2011). In section 4, we investigate the effect of the magnetic field and its degeneracy. We show that by studying only the high energy emission from the cascades, the magnetic field can not be determined, and additional constraints are needed from the synchrotron emission component. This is illustrated for the case of NGC 1275. In section 5, we will demonstrate that for moderately strong magnetic fields the synchrotron emission from the cascades can produce a signature resembling the big blue bump (BBB) observed in several blazars and demonstrate that this may make a non-negligible contribution to UV – soft X-ray SED. We illustrate this for the case of 3C 279. We summarize in Section 6.

## 2. Model Setup and Code Description

The general model setup used for this work is described in Roustazadeh & Böttcher (2010, 2011). The primary VHE  $\gamma$ -ray emission is represented as a mono-directional beam of  $\gamma$ -rays propagating along the X axis, described by a power-law with photon spectral index  $\alpha$  and a high-energy cut-off at  $E_{\gamma,max}$ . We assume that the primary  $\gamma$ -rays interact via  $\gamma\gamma$  absorption and pair production with an isotropic radiation field with arbitrary spectrum within a fixed boundary, given by a radius  $R_{ext}$ .

The assumption of an isotropic external radiation field is appropriate for line emission from the BLR, for distances from the central engine comparable to the size of the BLR ( $\sim 10^{17} - 10^{18}$  cm), and for infrared emission from cold dust in the nuclear environment, on typical scales of  $\sim$  parsec. Close to the central black hole and accretion disk, direct emission from the accretion disk may dominate the radiation energy density. However, for moderate distances from the disk, the primary  $\gamma$ -ray beam will interact with the accretion disk emission under an unfavorable angle for  $\gamma\gamma$  pair production. To illustrate this point, we plot in Figure 1 the opacity to  $\gamma\gamma$  absorption in the radiation field of an optically thick, geometrically thin

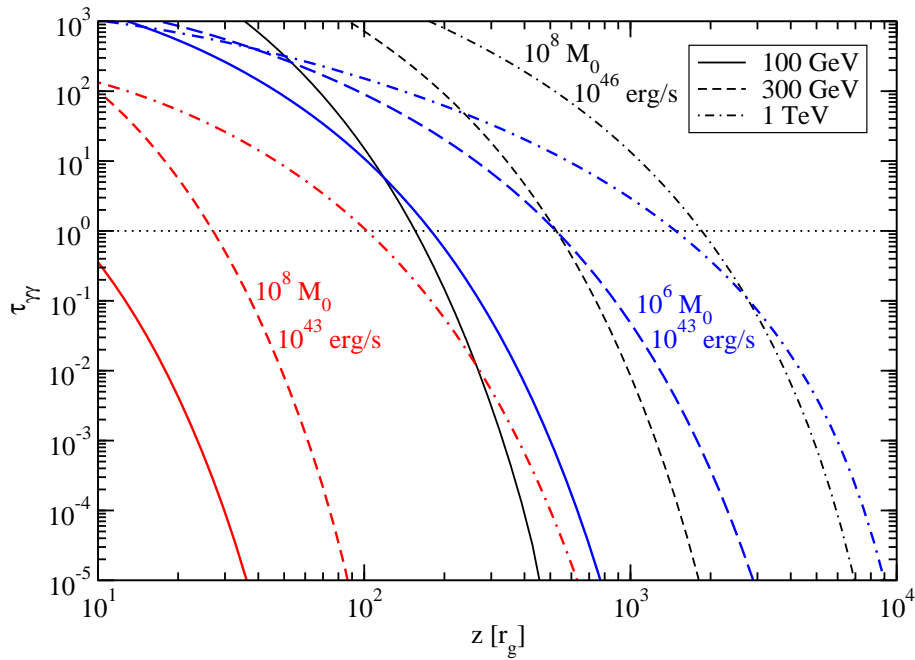


Fig. 1.—  $\gamma\gamma$  opacity due to accretion disk photons as a function of height  $z$  (in units of gravitational radii  $r_g = GM/c^2$ ) of the emission region above the black hole, for three different VHE  $\gamma$ -ray photon energies, and different black-hole masses and disk luminosities.

(Shakura & Sunyaev 1973) accretion disk as a function of height  $z$  of the emission region from the black hole. The figure shows that typically, the accretion-disk  $\gamma\gamma$  opacity drops below one at distances of a few  $100 - 10^3 r_g$  from the black hole. This is of the order of the characteristic height of the emission region in leptonic models of blazar emission, and much smaller than the size of the BLR or the dust torus. We therefore conclude that the neglect of the accretion-disk emission in our simulations is a good approximation throughout almost all of our simulation volume. For the case of thermal blackbody radiation fields considered below, we choose energy densities and blackbody temperatures characteristic of the observed properties (temperatures and total luminosities) of thermal infrared emission seen in AGN. In order to keep our treatment as model independent as possible, we do not specify the physical origin of the primary VHE  $\gamma$ -ray spectrum. The simplest assumption consistent with most models of  $\gamma$ -ray emission in blazars is a simple power-law, which we use as input spectrum in our simulations. The shape of the resulting pair cascade emission is only very weakly dependent on the exact shape of the incident VHE  $\gamma$ -ray spectrum. This is illustrated in Figure 2, in which we run a cascade simulation, once with a straight power-law, once with

a powerlaw + exponential cut-off (as a more realistic representation of a physical blazar high-energy spectrum), with identical environmental parameters, as listed in the figure caption. While the overall normalization of the cascade spectrum, obviously, depends on the flux of absorbed VHE  $\gamma$ -rays (which is higher in the pure power-law case), the cascade spectra at energies below the  $\gamma\gamma$  absorption trough are virtually identical. In the cases relevant for this study, only a small fraction of the  $\gamma$ -ray power is absorbed and re-processed into cascades. Therefore, feedback between the primary  $\gamma$ -ray production region and the cascade emission may be neglected, and the cascade development can be treated as a process separate from the (unspecified) VHE  $\gamma$ -ray production mechanism.

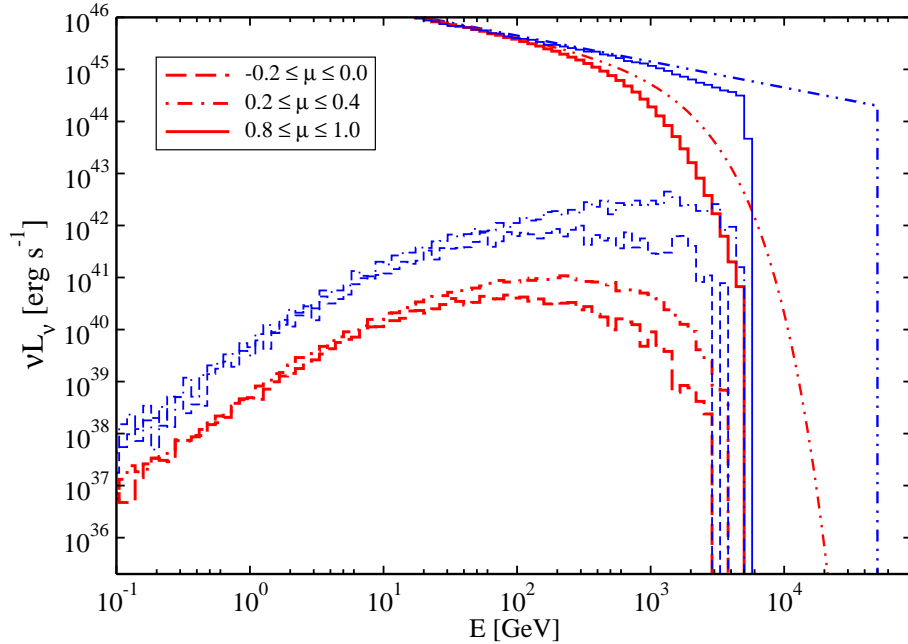


Fig. 2.— Comparison of the Compton emission from cascades for two different input VHE  $\gamma$ -ray spectral shapes: Blue (thin) lines indicate the emission for a pure power-law input spectrum; red (thick) lines for a power-law + exponential cut-off. Environmental parameters are the same as in Figure 3 (see below). Different line styles correspond to different viewing angles,  $\mu = \cos \theta_{\text{obs}}$ , with respect to the jet axis, as indicated in the legend. Parameters:  $B_x = B_y = 1 \mu\text{G}$ ,  $\theta_B = 45^\circ$ ;  $u_{\text{ext}} = 10^{-6} \text{ erg cm}^{-3}$ ,  $R_{\text{ext}} = 10^{18} \text{ cm}$ ,  $T = 1000 \text{ K}$ . The angular bin  $0.8 \leq \mu \leq 1$  contains the forward direction. The (unabsorbed) primary  $\gamma$ -ray input spectra are shown by the dot-dot-dashed lines.

Our code evaluates  $\gamma\gamma$  absorption and pair production using the full analytical solution

to the pair production spectrum of Böttcher & Schlickeiser (1997) under the assumption that the produced electron and positron travel initially along the direction of propagation of the incoming  $\gamma$ -ray. The trajectories of the particles are followed in full 3-D geometry. Compton scattering is evaluated using the head-on approximation, assuming that the scattered photon travels along the direction of motion of the electron/positron at the time of scattering. The Compton energy loss to the electron is properly accounted for at the time of each scattering.

For simplicity, the magnetic field in our simulations is treated as homogeneous, oriented at an angle  $\theta_B$  with respect to the jet axis. This may be considered an appropriate proxy for a helical magnetic field with the ratio of toroidal ( $B_{\text{tor}}$ ) and poloidal ( $B_x$ ) magnetic fields given by  $\tan \theta_B = B_{\text{tor}}/B_x$ . The code calculates the synchrotron energy loss of cascade particles in the following way: The energy of electrons/positrons is decreased by  $\Delta E_{\text{sy}} = \dot{E}_{\text{sy}} \frac{l_c}{c}$  between successive Compton scatterings, where  $l_c$  is the Monte Carlo generated distance traveled to the next scattering and  $\dot{E}_{\text{sy}} = -2c\sigma_T u_B \gamma^2 \sin^2 \psi$  with  $\psi$  being a pitch angle between the particle momentum and the magnetic field. We assume that the trajectory of the particles between two Compton scatterings is not affected by synchrotron radiation which is valid for  $u_B \lesssim u_{\text{ext}}$ . Then for 10 random points between two successive Compton scatterings, we determine the position and direction of motion of the particles at these points and write the spectral power in synchrotron radiation  $P_\nu$  into a synchrotron output file for the angular bin corresponding to the electron's/positron's direction of motion. The synchrotron power  $P_\nu$  of a single  $e^\pm$  is approximated as:

$$P_\nu = 2 \frac{c\sigma_T}{\Gamma(\frac{4}{3})} u_B \beta^2 \gamma^2 \frac{\nu^{1/3}}{\nu_c^{4/3}} e^{-\nu/\nu_c} \quad (1)$$

(Böttcher & Reimer 2012) where the critical frequency  $\nu_c = \frac{3qB}{4\pi m_e c} \gamma^2 \sin \psi = 4.2 \times 10^6 \sin \psi B_G \gamma^2$  Hz with  $B_G$  being the magnetic field in units of Gauss. The approximation (1) represents the synchrotron spectrum to within a few % at all frequencies.

### 3. Numerical Results

We have used the cascade Monte-Carlo code described in the previous section to evaluate the angle-dependent Compton and synchrotron spectra from VHE  $\gamma$ -ray induced pair cascades for a variety of generic parameter choices. Figure 3 illustrates the viewing angle dependence of the cascade emission. For this simulation, we assumed a magnetic field of  $B = \sqrt{2} \mu\text{G}$ , oriented at an angle  $\theta_B = 45^\circ$  with respect to the X axis ( $B_x = 1 \mu\text{G}$ ,  $B_y = 1 \mu\text{G}$ ). The external radiation field is a thermal blackbody with  $u_{\text{ext}} = 10^{-6}$  erg  $\text{cm}^{-3}$ ,

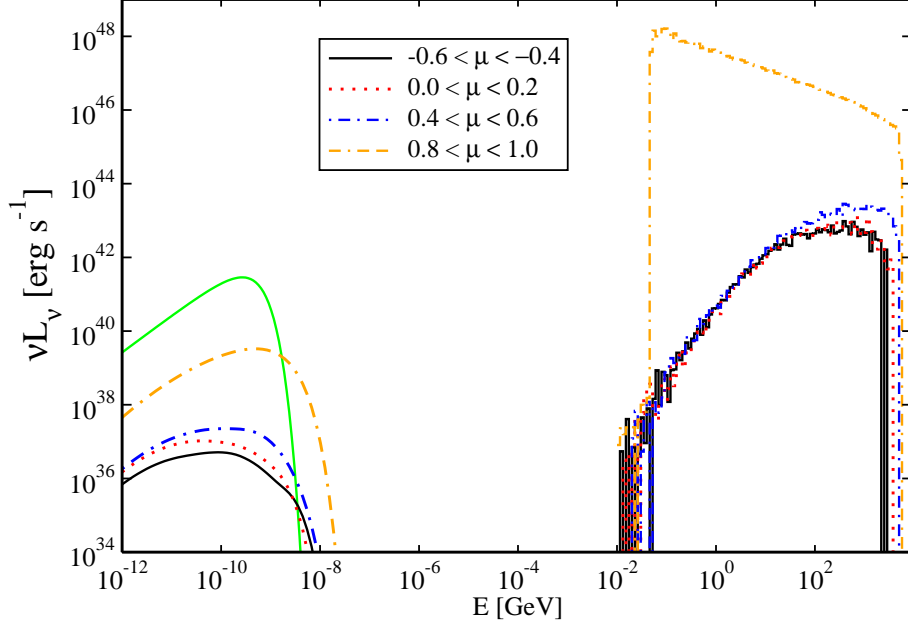


Fig. 3.— Cascade emission at different viewing angles ( $\mu = \cos\theta_{\text{obs}}$ ). Parameters of the target photon field are the same as for Figure 1. The input photon spectrum is a pure power-law with  $\alpha = 2.5$ ,  $E_{\gamma,\text{max}} = 5$  TeV. The green solid line represents the target photon field.

extended over a region of radius  $R_{\text{ext}} = 10^{18}$  cm, with a blackbody temperature of  $T = 10^3$  K (corresponding to a peak of the blackbody spectrum at a photon energy of  $E_s^{\text{pk}} = 0.25$  eV). This leads to a  $\gamma\gamma$  absorption cut-off at an energy  $E_c = (m_e c^2)^2 / E_s \sim 2$  TeV. The incident  $\gamma$ -ray spectrum has a photon index of  $\alpha = 2.5$  and extends out to  $E_{\gamma,\text{max}} = 5$  TeV.

For any given viewing angle  $\theta$  with respect to the direction of propagation of the primary  $\gamma$ -rays a critical electron energy for which the deflection angle over a Compton length equals the observing angle, i.e.,  $\theta \sim \lambda_{\text{IC}}/r_g$  can be defined. This yields the characteristic electron energy  $E_{e,\text{br}} = \gamma_c m_e c^2$  corresponding to a given observing angle  $\theta$ :

$$\gamma_c = \sqrt{\frac{3eB}{4\sigma_T u_{\text{ext}} \theta}} \sim 7.2 \times 10^5 B_{-6}^{1/2} u_{-3}^{-1/2} \theta^{-1/2} \quad (2)$$

where  $B_{-6} = B/\mu\text{G}$  and  $u_{-3} = u_{\text{ext}}/(10^{-3} \text{ erg cm}^{-3})$ .

This expression has been derived assuming that the Compton cooling length can be

calculated in the Thomson regime, which is valid for  $\gamma \lesssim 2 \times 10^6 T_3^{-1}$  for a thermal target photon field with temperature  $T = 10^3 T_3$  K, or  $\gamma \lesssim 5 \times 10^4$  for a Ly $\alpha$ -dominated target photon field. If these electrons radiate their energy by synchrotron radiation and Compton upscattering with the soft photon field in the Thomson regime, we can find the corresponding spectral breaks for synchrotron radiation and Compton scattering as a function of viewing angle:

$$E_{\text{sy,br}} \cong \gamma_c^2 B m_e c^2 / B_{\text{cr}} = \frac{3 m_e c^2 e B^2}{4 \sigma_T u_{\text{ext}} \theta B_{\text{cr}}} \sim 6.15 B_{-6}^2 u_{-3}^{-1} \theta^{-1} \text{meV} \quad (3)$$

$$E_{\text{IC,br}} \cong \gamma_c^2 E_s = \frac{3 e B}{4 \sigma_T u_{\text{ext}} \theta} E_s \sim 5.4 \times 10^2 E_{s,1} B_{-6} u_{-3}^{-1} \theta^{-1} \text{GeV}. \quad (4)$$

where the  $B_{\text{cr}} = \frac{m_e^2 c^3}{e \hbar} = 4.4 \times 10^{13} \text{G}$  and  $E_{s,1} = E_s / (1 \text{eV})$ .

Therefore, the ratio of the Compton to the synchrotron peak frequency is given by:

$$\frac{E_{\text{IC,br}}}{E_{\text{sy,br}}} = \epsilon_s \frac{B_{\text{cr}}}{B} \quad (5)$$

where  $\epsilon_s = \frac{E_s}{m_e c^2}$ .

Figure 3 shows that with increasing viewing angle, the spectral peaks of both the synchrotron and Compton emission shift to lower energy. This is because the Compton cooling length of the high energy particles is much smaller than their Larmor radius  $\lambda_{\text{IC}} \ll r_g$ , so they are emitting while traveling in the forward direction. Instead, for low energy particles,  $\lambda_{\text{IC}} \geq r_g$ , so that they are deflected before they are emitting. For the Compton emission this effect was already discussed in Roustazadeh & Böttcher (2010, 2011).

Figure 4 shows the cascade spectra for different values of the external radiation field energy density  $u_{\text{ext}}$ . In accordance with equations 3 and 4, for higher values of the external radiation field, the spectral breaks of both radiation components shift to lower energies. Figure 4 also shows that the synchrotron luminosities of the cascades decrease with increasing  $u_{\text{ext}}$  while the Compton luminosities of the cascades increase. For a larger value of  $u_{\text{ext}}$  and fixed blackbody temperature the soft target photon number density increases and  $\tau_{\gamma\gamma}$  becomes larger so that the number of VHE photons which will be absorbed increases and the photon flux of Compton emission from the cascades becomes larger. For very large values of  $u_{\text{ext}}$ ,  $\tau_{\gamma\gamma} \gg 1$  for photons above the pair production threshold so that essentially all VHE photons will be absorbed and the Compton flux from the cascade becomes independent of  $u_{\text{ext}}$  (Roustazadeh & Böttcher 2010, 2011). The ratio of emitted power in Compton to



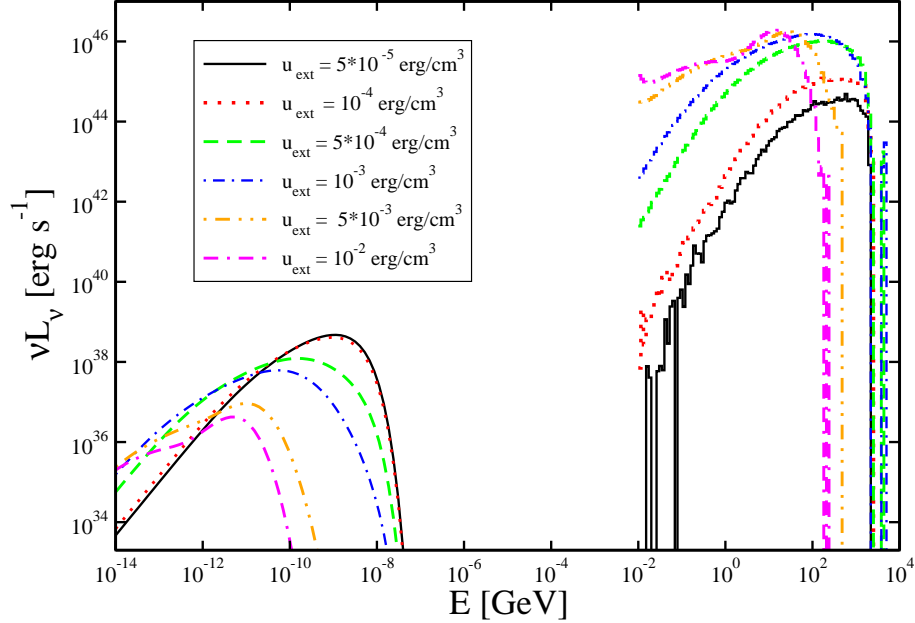


Fig. 4.— The effect of a varying external radiation energy density. Parameters:  $B_x = B_y = 10^{-6}$  G;  $R_{\text{ext}} = 10^{16}$  cm,  $T = 10^3$  K;  $\alpha = 2.5$ ,  $E_{\gamma, \text{max}} = 5$  TeV. The cascade emission in the angular bin  $0.2 \leq \mu \leq 0.4$  is shown.

synchrotron radiation in the linear regime ( $\tau_{\gamma\gamma} \lesssim 1$ ) is given by:

$$\frac{P_{sy}}{P_{IC}} = \frac{B^2/8\pi}{u_{\text{ext}}} \quad (6)$$

if Compton scattering occurs in the Thomson regime. The flux ratio  $\frac{F_{sy}}{F_{IC}} \propto u_{\text{ext}}^{-1}$ , so that by increasing the  $u_{\text{ext}}$  the synchrotron flux decreases.

Figure 5 illustrates the effect of a varying magnetic field strength for fixed magnetic field orientation ( $\theta_B = 45^\circ$ ). We see that the synchrotron peak energy increases proportional to the square of the magnetic field strength as expected from Eq. 3. As already discussed in Roustazadeh & Böttcher (2010, 2011) the Compton energy break is proportional to the magnetic field strength, as long as it occurs below the  $\gamma\gamma$  absorption cut-off energy. The synchrotron flux is proportional to the square of the magnetic field strength. The flux ratio is  $\frac{F_{sy}}{F_{IC}} \propto B^2$  until the fluxes become comparable, at which point our treatment of synchrotron losses breaks down.

Figure 6 illustrates the effects of a varying magnetic-field orientation with respect to

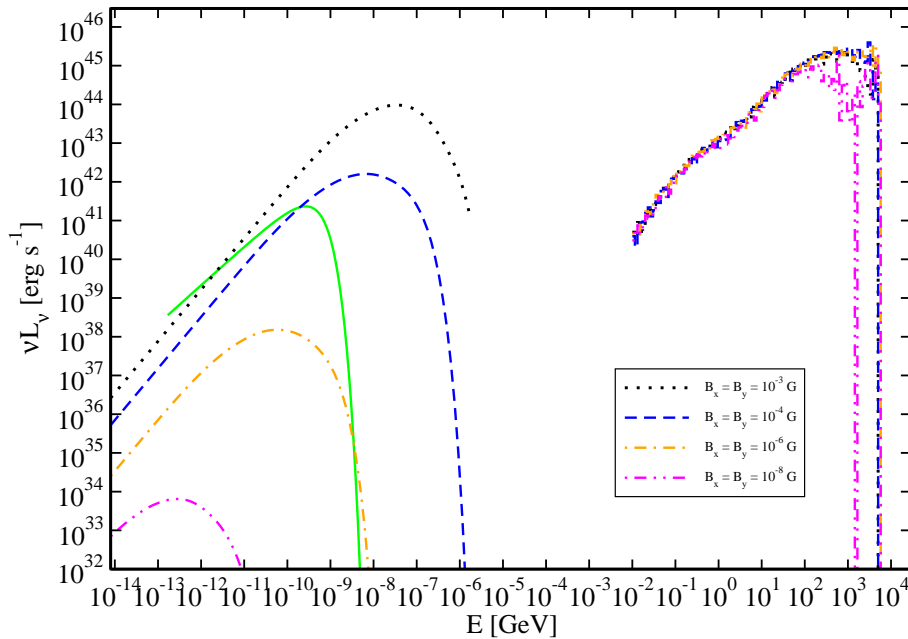


Fig. 5.— The effect of a varying magnetic field strength for a fixed angle of  $\theta_B = 45^\circ$  between jet axis and magnetic field. Parameters:  $u_{\text{ext}} = 10^{-6} \text{ erg cm}^{-3}$ ,  $R_{\text{ext}} = 10^{18} \text{ cm}$ ,  $T = 1000 \text{ K}$ ,  $\alpha = 2.5$ ,  $E_{\gamma, \text{max}} = 5 \text{ TeV}$ . The cascade emission in the angular bin  $0.2 \leq \mu \leq 0.4$  is shown. The solid green line represents the target photon field.

the jet axis, for fixed magnetic-field strength  $B = 1 \mu\text{G}$  for different angular bins. The results for the Compton component have been discussed Roustazadeh & Böttcher (2011). The figure illustrates that primarily the perpendicular ( $B_y$ ) component of the magnetic field is responsible for synchrotron radiation.

Figures 7 illustrate that the cascades emissions from the synchrotron radiation for parameters used in (Roustazadeh & Böttcher 2010, 2011) are negligible compared to the cascade Compton emission and much smaller than the synchrotron radiation from the jet itself. This confirms that neglecting synchrotron radiation in our previous works was justified.

#### 4. Magnetic Field degeneracy

In Roustazadeh & Böttcher (2010), we presented a fit to the *Fermi* spectrum of the radio galaxy NGC 1275. We now show that there is a degeneracy of the magnetic field,

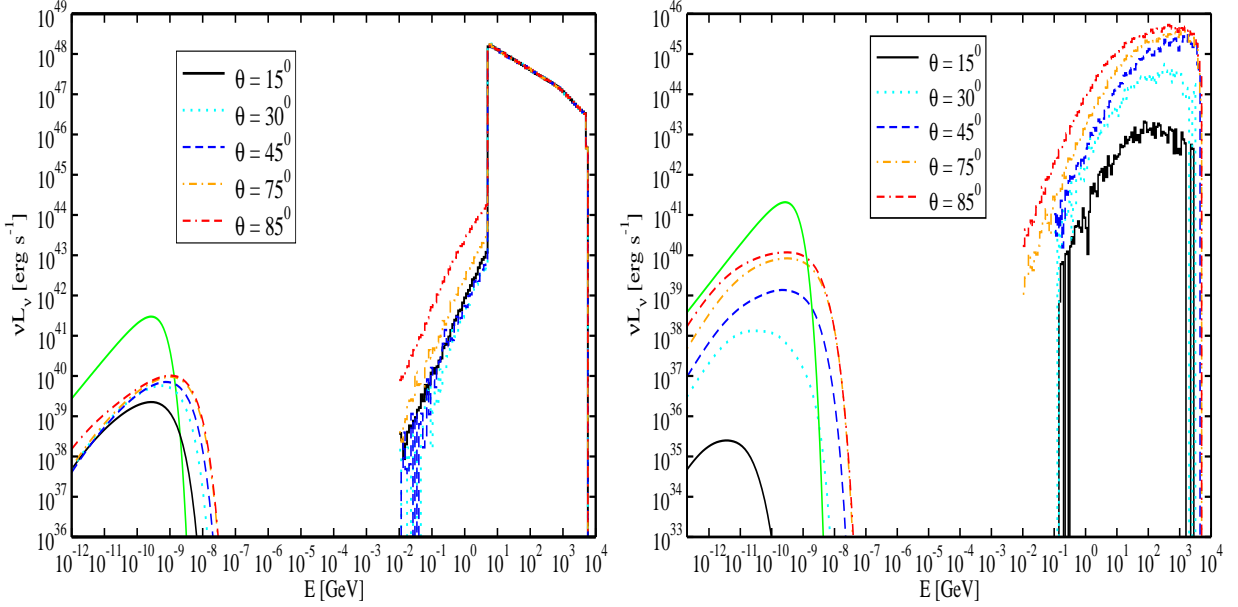


Fig. 6.— The effect of a varying magnetic field orientation for a fixed magnetic field strength of  $B = 1 \mu\text{G}$ ,  $u_{\text{ext}} = 10^{-6} \text{ erg cm}^{-3}$ ,  $R_{\text{ext}} = 10^{18} \text{ cm}$ ,  $T = 1000 \text{ K}$ ,  $\alpha = 2.5$ ,  $E_{\gamma, \text{max}} = 5 \text{ TeV}$ . Left figure: angular bin  $0.8 \leq \mu \leq 1.0$  (dominated by the forward direction, i.e., the blazar case). Right figure: angular bin  $0.2 \leq \mu \leq 0.4$ , representative of radio galaxies. The green solid lines represent the target photon fields.

both orientation and strength, if only the high energy output from the cascades is considered. Figure 8 shows this effect for NGC 1275. In this plot, the external radiation field is parameterized through  $u_{\text{ext}} = 5 \times 10^{-2} \text{ erg cm}^{-3}$  with photon energy  $E_s = E_{Ly\alpha}$  and  $R_{\text{ext}} = 10^{16} \text{ cm}$ . This size scale is appropriate for low-luminosity AGN as observed in NGC 1275 (e.g. Kaspi et al. 2007), and the parameters combine to a BLR luminosity of  $L_{\text{BLR}} = 4\pi R_{\text{ext}}^2 c u_{\text{ext}} = 1.9 \times 10^{42} \text{ erg s}^{-1}$ , in agreement with the observed value for NGC 1275. The magnetic field orientation is at an angle of  $\theta_B = 11^\circ$ . The mass of the black hole in NGC 1275 is uncertain, and estimates range from a few times  $10^6 M_\odot$  (Levinson et al. 1995) to  $\sim 10^8 M_\odot$  (Wilman et al. 2005). Assuming a characteristic fraction of 0.1 of the accretion-disk luminosity to be re-processed in the BLR, the accretion-disk luminosity may be estimated to be  $L_D \sim 10^{43} \text{ erg s}^{-1}$ . Figure 1 shows the  $\gamma\gamma$  absorption depth due to the disk radiation field for  $L_D = 10^{43} \text{ erg s}^{-1}$  for the two possible extreme values of the black-hole mass, as a function of height  $z$  of the emission region above the accretion disk. It shows that for  $M_{\text{BH}} = 10^6 M_\odot$ , the  $\gamma\gamma$  opacity drops below one at  $\sim 10^3 r_g \sim 10^{14} \text{ cm}$  from the black hole, while for  $M_{\text{BH}} = 10^8 M_\odot$   $\gamma\gamma$  absorption becomes negligible at  $\sim 10^2 r_g \sim 10^{15} \text{ cm}$

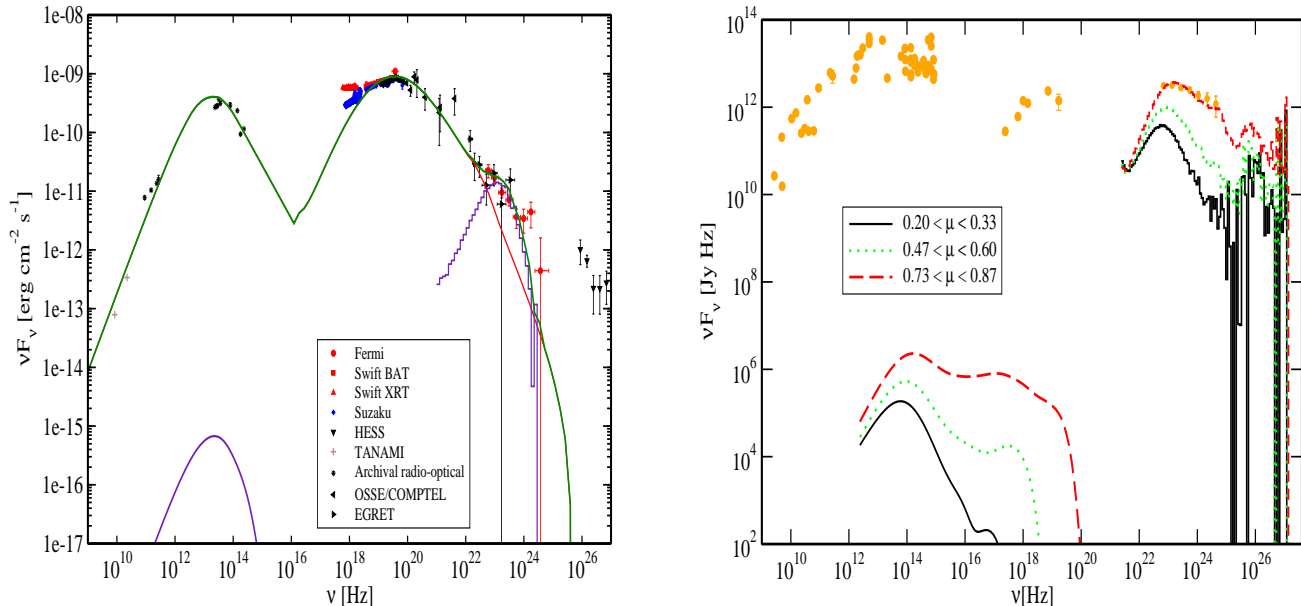


Fig. 7.— Compton and synchrotron radiation from the cascades. Left figure: (Fit to the SED of Cen A.); Right figure: (spectrum of NGC 1275 with a simulated cascade spectrum from a mis-aligned blazar, along with the cascade spectra at larger viewing angles)

for primary  $\gamma$ -rays of  $E_\gamma = 1$  TeV, and much earlier for lower-energy photons. Therefore, throughout most of our simulation volume ( $R_{\text{ext}} = 10^{16}$  cm),  $\gamma\gamma$  absorption in the disk radiation field can be safely neglected.

The cascade spectrum shown in Figure 8 pertains to the angular bin  $0.6 < \mu < 0.8$  (corresponding to  $37^\circ \lesssim \theta \lesssim 53^\circ$ ), appropriate for the known orientation of NGC 1275. In (Roustazadeh & Böttcher 2010, 2011), we have shown that for magnetic field values of  $B \geq 1$  nG and for energy density  $u_{\text{ext}} \geq 10^{-3}$  erg cm<sup>-3</sup>, there is no pronounced break in the cascade spectrum and the cascade is independent of magnetic field. In general we expect no break in the cascade Compton emission if  $E_{\text{IC,br}} \gtrsim \frac{(m_e c^2)^2}{E_s}$ , which leads to the condition:

$$B \gtrsim \frac{(m_e c^2)^2 4\sigma_T u_{\text{ext}} \theta}{3e(E_s)^2} \sim 5 u_{\text{ext},-3} E_{s,1}^{-2} \theta \text{ nG} \quad (7)$$

Figure 8 shows that while the high energy emission due to deflection of the cascade up to the  $\gamma\gamma$  absorption trough remains the same for the different magnetic fields, the synchrotron emission from the cascade changes. Therefore, determining the B field requires knowledge

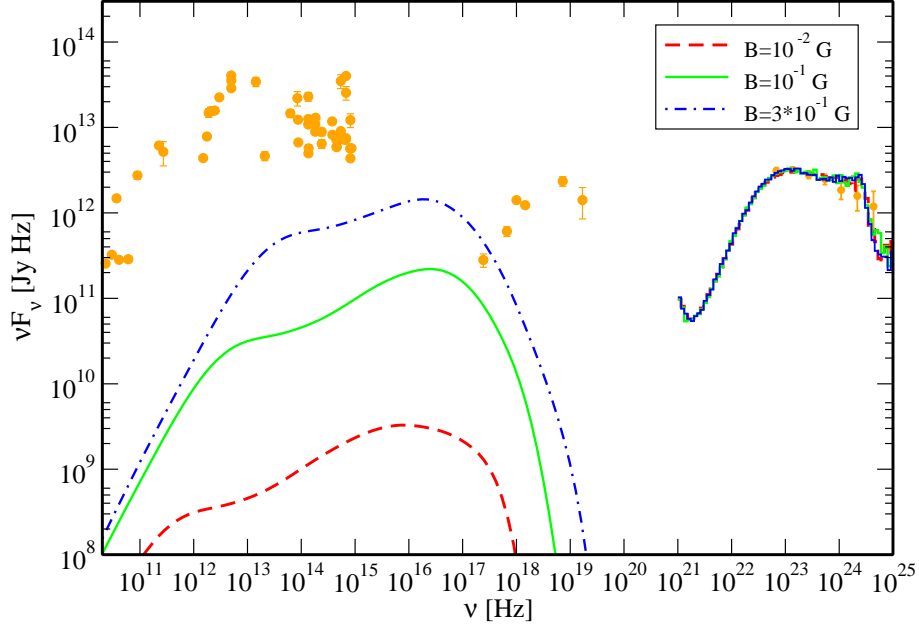


Fig. 8.— Synchrotron and Compton emission from the cascades for NGC 1275 ( $0.6 \leq \mu \leq 0.8$ ). Parameters:  $\theta_B = 11^\circ$ ;  $u_{\text{ext}} = 5 \times 10^{-2} \text{ erg cm}^{-3}$ ,  $R_{\text{ext}} = 10^{16} \text{ cm}$ ,  $E_s = E_{L\alpha}$ ,  $\alpha = 2.5$ ,  $E_{\gamma, \text{max}} = 5 \text{ TeV}$ .

of the synchrotron emission.

In the regime where  $E_{\text{IC,br}}$  is independent of the magnetic field,  $\nu_{\text{sy}} \propto B$  according to Eq. 5 and the synchrotron power is proportional to the square of magnetic field in agreement with figure 8.

Since the synchrotron/Compton flux ratio  $\frac{F_{\text{sy}}}{F_{\text{IC}}} \propto B^2$ , we expect that for sufficiently high magnetic fields, we will reach the regime where the Compton flux from the cascades is equal to or smaller than the synchrotron flux in which case our numerical scheme is no longer applicable.

## 5. The Big Blue Bump

The spectral Energy distribution of AGN in the ultraviolet (UV) to soft X-ray band ( $\sim 10 \text{ eV}$ - $1 \text{ keV}$ ) is notoriously difficult to observe because of dust and gas in our galaxy and

the AGN environment. The SEDs of many blazars exhibits a UV soft X-ray excess, called the big blue bump (BBB) (Pian et al 1999; Palma et al. 2011; Raiteri et al 2005, 2006, 2007). It is often attributed to the thermal emission from the accretion disk. In blazars, its signature is often particularly hard to detect because of dominant non-thermal emission from the jet. Understanding the origin of the BBB is important since this provides information on the central engine of the AGN.

3C 279 was among the first blazars discovered as a  $\gamma$ -ray source with the Compton Gamma-Ray Observatory (Hartman et al. 1992). In 2007 it was detected as a VHE  $\gamma$ -ray source with the MAGIC I telescope, making it the most distant known VHE  $\gamma$ -ray source at a redshift of 0.536 (Hewitt & Burbidge 1993). Its relativistic jet is oriented at a small angle to the line of the sight of  $< 0.5^\circ$  (Jorstad et al. 2004). It is also detected by *Fermi* (Abdo et al. 2009) with photon spectral index 2.23. There is evidence of a spectral break of around a few GeV to a photon spectral index of 2.50. It is strongly believed that the radio to optical emission is due to synchrotron radiation by relativistic particles in the jet. However, the origin of the high energy emission is still not well understood (see, e.g., Böttcher et al 2009).

Pian et al (1999) monitored 3C 279 in the ultraviolet, using IUE, and combined their data with higher-energy observations from ROSAT and EGRET from 1992 December to 1993 January. During this period, the source was in a very low state, allowing for the detection of a UV excess (the BBB), which is typically hidden below a dominant power-law continuum attributed to non-thermal emission from the jet. Pian et al (1999) proposed that the  $\gamma$ -ray emission in the SED of 3C 279 is produced by the external Compton mechanism, and suggested that the observed UV excess might be due to thermal emission from an accretion disk.

As an alternative to thermal emission from the accretion disk, Sikora et. al (1997) proposed the bulk Compton mechanism as a possible explanation of a UV/X-ray excess in quasar SEDs. If the jet contains a substantial population of cold (i.e., thermal, non-relativistic or mildly relativistic) electrons, they could scatter external optical/UV photons with the bulk Lorentz factor of  $\Gamma \sim 10$ , resulting in bulk Compton radiation in the far UV or soft X-ray range.

Here we suggest an alternative contribution to the BBB feature from cascade synchrotron emission. Figures 2 – 4 illustrate that the synchrotron emission from cascades may peak in the UV/X-ray range, thus mimicking a BBB for sufficiently strong magnetic fields ( $B \gtrsim 1$  mG). Figure 9 illustrates the contribution that synchrotron emission from VHE  $\gamma$ -ray induced pair cascades can make to the BBB in 3C 279. The primary HE  $\gamma$ -ray spectrum with a photon spectral index of  $\alpha = 2.5$  matcheds the Fermi spectrum of 3C 279. The external

radiation field is parameterized through  $u_{\text{ext}} = 10^{-4} \text{ erg cm}^{-3}$  and  $R_{\text{ext}} = 5 \times 10^{17} \text{ cm}$ , and the parameters combine to the luminosity of  $L = 4\pi R_{\text{ext}}^2 c u_{\text{ext}} \sim 10^{43} \text{ erg s}^{-1}$  corresponding to a  $\nu F_\nu$  peak flux of  $\sim 10^9 \text{ Jy Hz}$ , about 2 orders of magnitude below the observed IR/optical – UV flux level. The magnetic field is  $B = 10^{-2} \text{ G}$ , oriented at an angle of  $\theta_B = 85^\circ$ . The incident  $\gamma$ -ray spectrum extends out to  $E_{\gamma, \text{max}} = 5 \text{ TeV}$ , and the external radiation field is modeled as a blackbody with a temperature of  $T = 2000 \text{ K}$  (corresponding to a peak of the blackbody spectrum at a photon energy of  $E_s^{\text{pk}} = 0.5 \text{ eV}$ ). This leads to a  $\gamma\gamma$  absorption cut-off at an energy  $E_c = (m_e c^2)^2 / E_s \sim 1 \text{ TeV}$ .

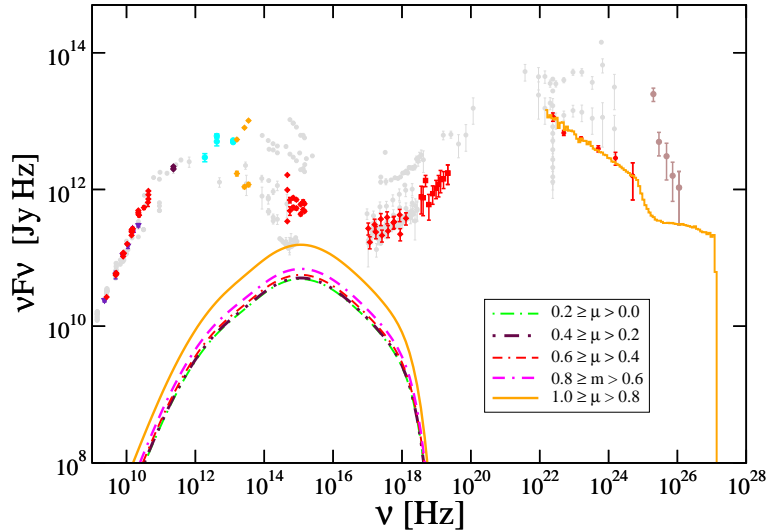


Fig. 9.— Illustration of a possible BBB in 3C 279 from cascade synchrotron emission. Parameters:  $B = 10^{-2} \text{ G}$ ,  $\theta_B = 85^\circ$ ;  $R_{\text{ext}} = 5 \times 10^{17} \text{ cm}$ ,  $T = 2000 \text{ K}$ ,  $\alpha = 2.37$ ,  $u_{\text{ext}} = 10^{-4} \text{ erg cm}^{-3}$ ,  $E_{\gamma, \text{max}} = 5 \text{ TeV}$ . Data from Abdo et al. (2010).

We suggest that synchrotron emission from VHE  $\gamma$ -ray induced pair cascades can enhance the BBB feature in the SEDs of several blazars such as 3C 279. An observational test of this hypothesis may be provided through spectropolarimetry. A BBB due to (unpolarized) thermal emission from an accretion disk will produce a decreasing percentage of polarization with increasing frequency throughout the optical/UV range. In contrast, if the BBB is produced as synchrotron emission from cascade pairs in globally ordered magnetic fields, it is also expected to be polarized. Therefore, we predict that a BBB due to cascade synchrotron emission would result in a degree of polarization showing only a weak dependence on frequency over the optical/UV range. As an example, in recent observations of the high-redshift  $\gamma$ -ray loud quasar PKS 0528+134, Palma et al. (2011) found a decreasing

degree of polarization with increasing frequency throughout the optical range, arguing for an increasing contribution from thermal emission towards the blue end of the optical spectrum.

## 6. Summary

We investigated the magnetic-field dependence and synchrotron emission signatures of Compton-supported pair cascades initiated by the interaction of nuclear VHE  $\gamma$ -rays with arbitrary external radiation fields, for a model-independent, generic power-law shape of the primary VHE  $\gamma$ -ray emission. We follow the spatial development of the cascade in full 3-dimensional geometry and study the dependence of the radiative output on various parameters pertaining to the external radiation field and the magnetic field in the cascade region. We confirm that synchrotron radiation from the cascades is negligible in NGC 1275 and Cen A for the parameters we used in our previous works. We demonstrated that the magnetic field can not be well constrained by considering the high-energy (Compton) output from the cascade emission alone, without observational signatures from their synchrotron emission. This was illustrated for the case of NGC 1275, for which we could produce equally acceptable fits to the Fermi spectrum for a variety of magnetic-field values, which resulted in substantially different synchrotron signatures.

We have shown that synchrotron emission from VHE  $\gamma$ -ray induced pair cascades may produce UV/X-ray signatures resembling the BBB observed in the SEDs of several blazars, in particular in their low states. We used the example of 3C 279 to illustrate that cascade synchrotron emission may make a substantial contribution to the BBB feature. We point out that spectropolarimetry may serve as a possible observational test to distinguish a thermal from a non-thermal (cascade) origin of the BBB.

This work was supported by NASA through Fermi Guest Investigator Grants NNX09AT81G and NNX10AO49G. We thank the anonymous referee for valuable suggestions.

## REFERENCES

- Abdo, A. A., et al., 2009, ApJ, 700, 597
- Abdo, A. A., et al., 2010, ApJ, 716, 30
- Abdo, A. A., et al., 2011, ApJ, 726, 43
- Acciari, V. A., et al., 2008, ApJ, 684, L73



- Aharonian, F. A., Khangulyan, D., & Costamante, L., 2008, *MNRAS*, 387, 1206
- Bednarek, W., & Kirk, J. G., 1995, *A&A*, 294, 366
- Böttcher, M., Reimer, A., & Marscher, A. P., 2009, *ApJ*, 703, 1168
- Böttcher, M., & Bloom, S. D., 2000, *AJ*, 119, 469
- Böttcher, M., & Schlickeiser, R., 1997, *A&A*, 325, 866
- Böttcher, M., & Reimer, A., 2012, Chapter 3, “Radiation Processes”, in “Relativistic Jets from Active Galactic Nuclei”, Eds. M. Böttcher, D. Harris, & H. Krawczynski, Wiley-VCH, 2012
- Donea, A. C., & Protheroe, R. J., 2003, *Astrop. Phys.*, 18, 337
- Ghisellini, G., et al., 1998, *MNRAS*, 301, 451
- Hartman, R. C., et al., 1992, *ApJ* 385L, 1
- Hewitt, A. & Burbidge G., 1993, *ApJS*, 87, 451 3
- Jorstad, S. G., et. al., 2004, *AJ*. 127, 3115
- Kaspi, S., Brandt, W. N., Maoz, D., Netzer, H., Schneider, D. P., & Shemmer, O., 2007, *ApJ*, 659, 997
- Levinson, A., Laor, A., & Vermeulen, R. C., 1995, *ApJ*, 448, 589
- Liu, H. T., Bai, J. M., & Ma, L., 2008, *ApJ*, 688, 148
- Madejski, G. M., et al., 1999, *ApJ*, 521, 145
- Palma, N., et al, 2011, *ApJ*, 735, 60
- Piam, E., at al, 1999, *ApJ*, 521, 111
- Poutanen, J., & Stern, B., 2010, *ApJ*, 717, L118
- Protheroe, R. J., & Biermann, P. L., 1997, *Astrop. Phys.*, 6, 293
- Raiteri, C. M., at al, 2005, *A&A*, 438, 39
- Raiteri, C. M., at al, 2006, *A&A*, 452, 845
- Raiteri, C. M., at al, 2007, *A&A*, 473, 819

- Reimer, A., 2007, *ApJ*, 665, 1023
- Roustazadeh, P., & Böttcher, M., 2010, *ApJ*, 717, 468
- Roustazadeh, P., & Böttcher, M., 2011, *ApJ*, 728, 134
- Shakura, N. I., & Sunyaev, R. A., 1973, *A&A*, 24, 337
- Sikora, M., Madejski, G., Moderski, R. & Poutanen, J., 1997, *ApJ*, 484, 108
- Sitarek, J., & Bednarek, W., 2008, *MNRAS*, 391, 624
- Sitarek, J., & Bednarek, W., 2010, *MNRAS*, 401, 1983
- Urry, C. M., & Padovani, P., 1995, *PASP*, 107, 803
- Vermeulen, R. C., et al., 1995, *ApJ*, 452, L5
- Wilman, R. J., Edge, A. C., & Johnstone, R. M., 2005, *MNRAS*, 359, 755